

Leveraging Multi-Modal Saliency and Fusion for Gaze Target Detection

Athul M. Mathew

AMATHEW@ELM.SA

Arshad Ali Khan

ARKHAN@ELM.SA

Thariq Khalid

TKADAVIL@ELM.SA

Faroq AL-Tam

FALTAM@ELM.SA

Riad Souissi

RSOUSSI@ELM.SA

Elm Company, Saudi Arabia

Abstract

Gaze target detection (GTD) is the task of predicting where a person in an image is looking. This is a challenging task, as it requires the ability to understand the relationship between the person’s head, body, and eyes, as well as the surrounding environment. In this paper, we propose a novel method for GTD that fuses multiple pieces of information extracted from an image. First, we project the 2D image into a 3D representation using monocular depth estimation. We then extract a depth-infused saliency module map, which highlights the most salient (*attention-grabbing*) regions in image for the subject in consideration. We also extract face and depth modalities from the image, and finally fuse all the extracted modalities to identify the gaze target. We quantitatively evaluated our method, including the ablation analysis on three publicly available datasets, namely VideoAttentionTarget, GazeFollow and GOO-Real, and showed that it outperforms other state-of-the-art methods. This suggests that our method is a promising new approach for GTD.

Keywords: gaze target detection, gaze-following, 3D gaze, free-viewing, saliency, depth map, 3D projection, point cloud, multi-modal, fusion

1. Introduction

It is general phenomenon that human gaze acts as a natural cue which provides rich contextual information on the attention of individuals when it comes to social interactions, engagements and communication. Gaze is a fundamental human communication mean, since it can express emotions, feelings, and intentions (Lund, 2007). Human beings have a remarkable capability to follow the gaze of others to understand their gaze target, understand whether a person is gazing at them and determine the attention of others (Chong et al., 2018). GTD, also known as *gaze-following*, is an active research area and can have a wide range of applications, including human-computer interaction, educational assessment, treatment of patients with cognitive or neurological disorders such as early diagnosis of ADHD (Attention Deficit Hyperactivity Disorder) in children and so on.

Gaze estimation (GE) utilizes eye or facial images of a person to estimate the direction of gaze for the person (Huang et al., 2017) (Krafka et al., 2016). These methods utilize facial features of the person, such as the eyes, nose, and mouth, to estimate the three-dimensional orientation (i.e. *Yaw*, *Pitch* and *Roll*) of the face and predict the gaze direction. These methods can be less accurate, especially in challenging conditions such as low lighting or when the person is wearing glasses. Typical gaze detection and tracking systems often

require a calibration step, where the user is asked to look at various points before usage of such a system. Also, such gaze tracking systems are constrained because they are designed to monitor the gaze of one person when the person is well situated within the confined space of monitoring for the gaze tracking system. An example of such a system is a driver attention or fatigue detection system in vehicles where the system is expected to monitor the gaze of the driver seated on the driving seat.

Unlike GE, the GTD of a given person in an image involves learning relationship between the relative position of the person within the scene and the surrounding objects that lie within the field-of-view of that person. A robust and scalable gaze target assessment system is needed to identify the salient objects that people are likely looking at. While significant progress has been made in GTD from images, incorporating depth-related contextual cues remains a challenge. Such cues can enhance the accuracy and robustness of GTD, but reconstructing these cues from 2D images in multiple scenarios is difficult. This problem is further exacerbated when detecting the gaze target when the person is looking at a point on a smartphone screen (Zhang et al., 2015), or when predicting fixation on an object when the person is looking at a salient object within or outside the frame (Chong et al., 2020). In this paper, we focus on in-frame GTD due to time and scope constraints.

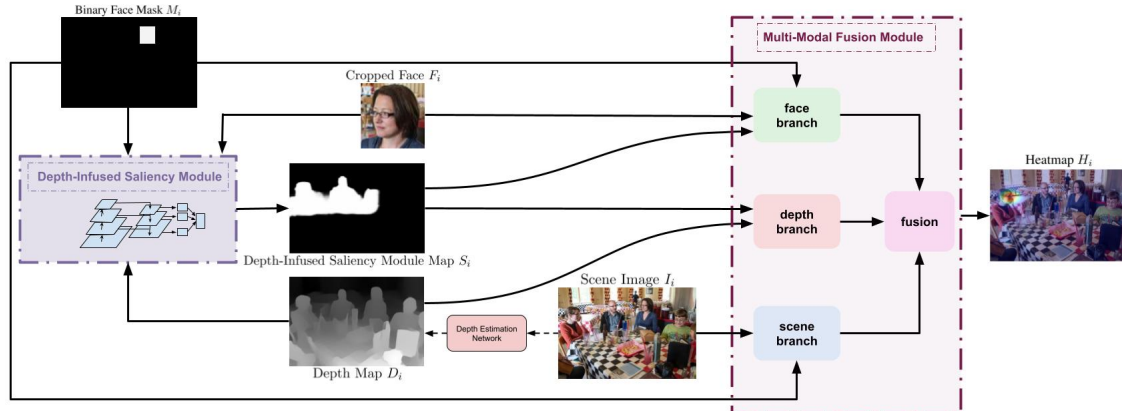


Figure 1: Overview of our multi-modal saliency and fusion architecture for gaze target detection.

Our GTD architecture consists of two modules, as shown in Figure 1. Firstly, **Depth-Infused Saliency Module** (DISM) extracts a map (binary mask) that highlights objects and artifacts that are in the line-of-sight of the subject’s gaze within the scene. This map is predicted from the scene features that lie along the subject’s field-of-view, based on contextual cues such as the subject’s depth and spatial positioning in the scene. The second module, **Multi-Modal Fusion** (MMF), blends the DISM map with rich representations of scene, depth, and head features. This fusion process creates a unified representation of the scene that incorporates information from multiple sources. Together, the two modules work together to infer the gaze fixation of a given subject within the image. We further elaborate this method in Section 3. It is important to mention that many visual-attention-based saliency models (Itti and Koch, 2001) (Judd et al., 2009) focus on identifying visual gaze fixations of a person *free-viewing* a natural image. In GTD, people in the picture might fixate on objects even when they are not the most salient (Recasens* et al., 2015). Our work

goes beyond this, since we learn gaze target with respect to a person’s viewpoint, and the learnt saliency map adapts based on the person’s location and facial orientation within the image. In this research, our network in DISM aims to identify salient scene artefacts specific to the person in consideration within the image and this may not necessarily be the *free-viewing* saliency. Additionally, our MMF module introduces dedicated attention layers to distill the learnt saliency across face, scene, and depth branches and fuses the multi-modal embeddings effectively. Such multimodal design leads to achieving better performance when compared to those presented in similar contemporary prior-art research.

The remainder of this paper is organized as follows: Section 2 reviews state-of-the-art GE and GTD methods. Section 3 lays out our methodology, including our proposed architecture for extraction of DISM map and MMF. Section 4 discusses extensive experimental results and evaluation against established benchmarks using Area Under the Curve (AUC), Distance and Angular metrics. In Section 5, we summarize our research findings and, Section 6 sets out our goals for extending this work in the future.

2. Related Work

The study of automatic gaze analysis can be divided into two categories: gaze estimation (GE) and gaze target detection (GTD) (Chong et al., 2020) (Fang et al., 2021) (Recasens et al., 2017). GE estimates the direction of a person’s gaze, typically in 3D, and does not necessarily focus on precisely locating the object of their interest (Zhang et al., 2018)(Guo et al., 2023). Methods such as Parks et al. (2015) estimate the gaze direction and do not identify the objects that are being attended to. On the other hand, Liu et al. (2020) uses a head-mounted eye-tracker to estimate the user’s point of gaze. Similarly Thakur et al. (2021) also elaborate a method to detect where each person in the scene is looking by fusing videos and Inertial Measurement Unit (IMU) data. However, both these methods focus on GTD from the first-person viewpoint. There have been significant developments in gaze and saliency mapping, but robust 3D gaze orientation determination is still a challenging problem. Chong et al. (2018) rely on a 3D gaze angle regression model for GTD. Subsequently, Chong et al. (2020) extends the work to include temporal information to directly output an estimate of gaze uncertainty. In this paper, we focus on GTD with in-the-wild images, captured from a third-person viewpoint.

GTD has been evolving given the adaptation of computer vision technologies in human gaze research. It has become evident that in domains where close-level iris/eye tracking is not possible, head pose is the most important feature for estimating human focus of attention, along with other semantic information. While modelling 3D gaze requires additional human annotations (Jin et al. (2022)), models trained on such datasets still struggle to generalize to common scenarios. Fang et al. (2021) have pinpointed three significant issues in previous research. Firstly, most research works explore the gaze direction in 2D representation without encoding the depth modality. Secondly, salient object searching from 2D visual cues without depth understanding. Finally, learning mapping functions directly from head position to gaze direction without considering the relationship between eyes and head. Thus a comprehensive understanding of 3D scenes is essential to identify candidate objects lying at different depth layers along the subject’s gaze direction.

While many approaches learn the mapping function from head features to gaze direction using 2D visual cues (Recasens* et al., 2015) (Chong et al., 2018) (Chong et al., 2020) (Recasens et al., 2017), estimating depth information from a RGB image is essential to accurately predicting the gaze target. Fang et al. (2021) and Tonini et al. (2022) introduced a dedicated depth branch to embed depth-related cues within their architecture. However, conventional depth estimation is a challenging task given the ill-posed nature of estimating real depth from a single RGB image. In the context of GTD, for example, using monocular depth estimation there may be multiple solutions in terms of estimating the distance from a viewpoint for a given target. Recently, deep neural networks have mitigated this problem by exploiting multiple visual cues such as relative size, brightness, patterns, and vanishing points extracted from an RGB image (Shim et al., 2023). New deep-learning frameworks for head localization and pose estimation on depth images are being used to tackle issues arising from poor illumination conditions, occlusion, and dynamic scenes (e.g., in low light and with illumination changes during the day). Moreover, Shim et al. (2023) propose a transformer-based approach called Relative Depth Transformer (RED-T), which uses relative depth as guidance in self-attention, such that the model assigns high attention weights to pixels of close depth and low attention weights to pixels of distant depth. However, transformer-based models typically require longer training and inference time than CNN counterparts, especially when a multimodal solution is adopted in the inference pipeline. Another challenge is the 3D reconstruction of the scene once the depth estimation is done, in order to place objects in 3D space and align them with their estimated depths.

Saliency mapping, in depth estimation, is another aspect that involves identifying and highlighting the most visually significant regions in a scene contributing to the depth perception element. Researchers like Recasens* et al. (2015) and Chong et al. (2020) present methods that completely discard utilization of depth modality within their networks which may prevent the GTD algorithms from identifying salient regions in a scene from the perspective of a human observer. Tonini et al. (2022) include a dedicated branch for depth modality, where the depth is processed as pixels in 2D image space. Fang et al. (2021) extract a depth-based attention map, however, they utilize only the coarse depth features for extraction of the saliency map.

One of the challenges, arising from integrating 2D annotation with 3D scene models for GTD is the semantic understanding and interaction with the scene. Bao et al. (2022) propose a GTD method that explicitly models 3D scenes using only 2D gaze annotations. Their research is particularly interesting because it considers 3D geometry to model the scene for GTD. However, this method assumes that the front-most object is always the salient object and this may not be valid at all times.

Tu et al. (2022) propose Human Gaze Target detection Transformer (HGTT), which simultaneously detects multiple human head locations and their associated gaze targets at once in an image (instead of salient object detection and gaze prediction separately). This approach is more computationally efficient than the traditional two-stage head location and gaze target detection pipeline. However, HGTT reports high false positives in images with a single human gaze target, making it less attractive for users evaluating gaze target detection datasets such as GazeFollow.

In terms of interesting real-world use cases, Senarath et al. (2022) proposed Retail Gaze, and Tomas et al. (2021) proposed GOO which are datasets for GTD in real-world retail

environments. There has also been some work in the context of classroom gaze measurement use-case. [Ahuja et al. \(2021\)](#) develop a new computer vision system that powers a 3D "digital twin" of the classroom. GTD is performed by post-processing the estimated gaze orientation of the face and ArUco markers ([Garrido-Jurado et al., 2014](#)) placed on objects around the classroom. Furthermore, [Ömer Sümer et al. \(2021\)](#) experimented with multimodal engagement analysis from facial videos in the classroom.

3. Our Methodology

Figure 1 outlines our method which extracts the DISM map S_i using depth map D_i , binary face mask M_i , and cropped face F_i . The scene image I_i along with other modalities D_i , F_i , M_i , S_i are fused to estimate the gaze target point of any given person in an image. Furthermore, our methodology has been clearly explained in Algorithm 1.

Algorithm 1: Method for Gaze Target Detection

Input: Image stream I_1, \dots, I_n
Output: Heatmap H_i
Given: Depth-Infused Saliency network f_{ds} , Scene Branch f_s , Depth Branch f_d ,
Face Branch f_f , Fusion Branch f_n
Function **Depth_Infused_Saliency**(D_i, M_i, F_i):
| **return** $S_i = f_{ds}(D_i, M_i, F_i)$
End Function
Function **Multi_Modal_Fusion**(S_i, I_i, D_i, M_i, F_i):
| **scene_features** = $f_s(\text{concatenate}(I_i, M_i))$
| **depth_features** = $f_d(\text{concatenate}(D_i, S_i))$
| **face_features** = $f_f(F_i)$
| **modulated_scene_features** = $\text{modulate_scene}(\text{scene_features}, \text{face_features}, S_i)$
| **modulated_depth_features** = $\text{modulate_depth}(\text{depth_features}, \text{face_features}, M_i)$
| **gaze_fixation** = $f_n(\text{modulated_scene_features}, \text{modulated_depth_features})$
| **return** **gaze_fixation**
End Function
Function **GazeTargetDetection**(I_i, D_i, M_i, F_i):
| $S_i = \text{Depth_Infused_Saliency}(D_i, M_i, F_i)$
| **gaze_fixation** = **Multi_Modal_Fusion**(S_i, I_i, D_i, M_i, F_i)
| **return** **gaze_fixation**
End Function
for $i \leftarrow 1$ **to** n **do**
| Extract D_i, M_i, F_i from I_i
| $H_i = \text{GazeTargetDetection}(I_i, D_i, M_i, F_i)$
end

3.1. Depth-infused Saliency Module (DISM)

The depth-infused saliency network, f_{ds} , uses a Feature Pyramid Network (FPN) architecture ([Lin et al., 2017](#)) to learn high-level semantic saliency for the subject of interest. The network takes a concatenated 7-channel input of the scene depth map D_i , binary head position mask M_i , and face image F_i . M_i and D_i encode the subject's relative three-dimensional position in the scene. F_i helps the model to focus on scene artefacts that lie along a projection plane originating from the subject's facial position along the depth axis and are directed parallel to the facial orientation vector. The network finally predicts a DISM map, S_i that highlights the most likely gaze fixation artefacts for the subject in the scene. An overview of the depth-infused saliency network f_{ds} is shown in Figure 2.

It is our intention to simplify the learning objective of DISM and utilize it to provide rich cues for the MMF module. We bin the human gaze direction θ along the depth plane θ_d into *forward* (θ_{df})(90°), *intermediate-forward* (θ_{dif})(45°), *same-plane* (θ_{ds})(0°), *intermediate-backward* (θ_{dib})(-45°) and *backward* (θ_{db})(-90°) directions. The gaze direction along the image plane θ_{xy} is binned into *lower-right* ($\theta_{xy_{lr}}$)(30°), *straight* (θ_{xy_s})(90°), *lower-left* ($\theta_{xy_{ll}}$)(150°), *upper-left* ($\theta_{xy_{ul}}$)(220°) and *upper-right* ($\theta_{xy_{ur}}$)(320°) directions. At any instance, the 3D-gaze angle will comprise an image plane component and a depth plane component. That is, $\theta = [\theta_{xy}, \theta_d]$, where $\theta_{xy} \in \{\theta_{xy_{lr}}, \theta_{xy_s}, \theta_{xy_{ll}}, \theta_{xy_{ul}}, \theta_{xy_{ur}}\}$ and $\theta_d \in \{\theta_{df}, \theta_{dif}, \theta_{ds}, \theta_{dib}, \theta_{db}\}$.

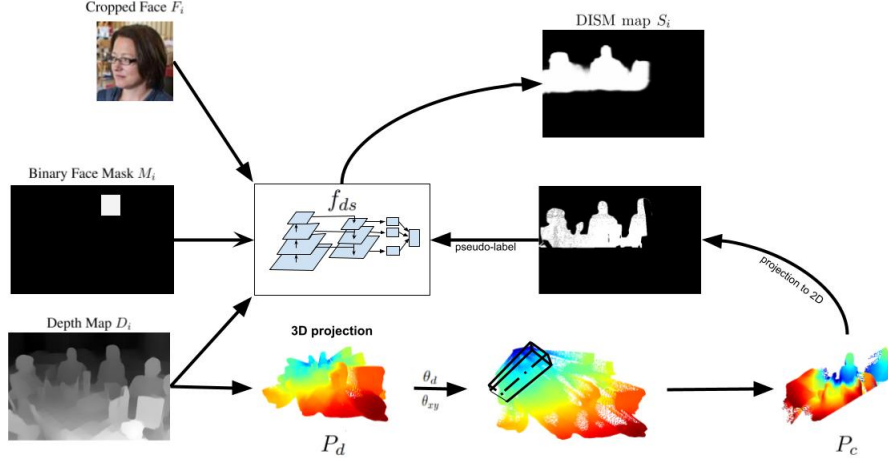


Figure 2: Overview of DISM. We take 3D projection of depth map P_d alongside gaze binning parameters θ_d and θ_{xy} to extract a sub-collection of filtered 3D points P_c . The re-projection of P_c back to the image-plane serves as pseudo-labels for the FPN network, f_{ds} . The network provides a representation of the learned DISM map S_i .

3.1.1. DATA PRE-PROCESSING

Pseudo-labels for DISM require relative depth between face and target point, computed using monocular depth estimation techniques such as [Ranftl et al. \(2020\)](#) and [Ranftl et al. \(2021\)](#). Depth plane gaze angle θ_d is extracted using average depth of face d_f and target points d_t , and empirically setting depth plane binning thresholds γ_1 and γ_2 to 3 and 10 respectively.

$$\theta_d = \begin{cases} \theta_{ds} & , \text{if } d_f - d_t < \gamma_1 \\ \theta_{dif} & , \text{if } \gamma_1 < d_f - d_t < \gamma_2 \\ \theta_{dib} & , \text{if } \gamma_1 < d_t - d_f < \gamma_2 \\ \theta_{df} & , \text{if } d_f - d_t > \gamma_2 \\ \theta_{db} & , \text{if } d_t - d_f > \gamma_2 \end{cases} \quad (1)$$

The gaze direction along the image plane θ_{xy} is extracted from the pixel positions of the eye (e_x, e_y) and the gaze target (g_x, g_y) . Given $\theta_{xy} \in \{\theta_{xy_{lr}}, \theta_{xy_s}, \theta_{xy_{ll}}, \theta_{xy_{ul}}, \theta_{xy_{ur}}\}$, the

image angle α is discretized which assumes one of the values within θ_{xy} . α is computed as:

$$\alpha = \arctan \frac{g_y - e_y}{g_x - e_x} \quad (2)$$

where the fraction calculates the gradient between the eye location and gaze fixation points.

3.1.2. DEPTH-INFUSED SALIENCY MAP

The dataset A comprises of N images such that $A = \{I_i, D_i, M_i, F_i\}_{i=1}^N$, where $I_i \in \mathbb{R}^{H_i \times W_i \times 3}$ is i -th image in the dataset. H_i and W_i denote the width and height of image. D_i is the depth map of I_i . The binary mask of the head position of the subject within the scene is denoted as M_i and F_i is the cropped face of the subject. The DISM map for all images is represented as $S = \{S_i\}_{i=1}^N = \{\{s_i^m\}_{m=1}^{H_i \times W_i}\}_{i=1}^N$ where $s_i^m \in \{0, 1\}$ denote presence of m -th pixel in DISM map of i -th image, with $m = [1, \dots, H_i \times W_i]$. We can represent the network f_{ds} which predicts the DISM map S_i as :

$$S_i = f_{ds}(D_i, M_i, F_i) \quad (3)$$

In order to extract the ground truth DISM map S_i (pseudo-labels), the depth map is projected onto a 3D grid representation using focal length (f_x, f_y) and optical centre (c_x, c_y) of the depth camera parameters from Places dataset. The extrinsic parameters are assumed to be an identity matrix. Let P_d be the collection of 3D projection points of the depth map D_i . For every pixel location (a, b) of the depth map, p is a point within the collection P_d such that :

$$p = \begin{cases} p_x = \frac{(j-c_x)D_i[a,b]}{f_x} \\ p_y = \frac{(i-c_y)D_i[a,b]}{f_y} \\ p_z = D_i[a,b] \end{cases} \quad (4)$$

A cuboid aligned along θ_{xy} in the XY plane and θ_d in the Z plane is projected from the face position in 3D space. The orientation of the 3D projection cuboid is determined using the image plane and depth plane gaze angle parameters θ_{xy} and θ_d obtained from Equation (1) and (2), respectively. P_c is the collection of 3D points within the volume of the projected cuboid, where $P_c \subset P_d$. The collection, P_c is then re-projected back to the image plane as a binary mask using the depth camera parameters to finally derive the DISM map S_i . The ground truth saliency mask, S_i , and prediction saliency mask, \hat{S}_i are trained with the objective of minimizing the Jaccard distance (JD). We have opted for JD as it is considered suitable for binary segmentation tasks or mask comparison, especially in our case where precise delineation of regions matters a lot. The metric provides normalized measures of IOU along with computational efficiency and interpretability benefits which allows for meaningful comparison across different scales. The objective function to minimize JD is given by L_j as :

$$L_j(S_i, \hat{S}_i) = 1 - \frac{(S_i \cdot \hat{S}_i) + \epsilon}{(S_i + \hat{S}_i - S_i \cdot \hat{S}_i) + \epsilon} \quad (5)$$

where ϵ prevents zero division.

Our method in DISM generates 3D point clouds and embeds complete 3D information when modelling the DISM map and makes no assumptions regarding the spatial relationship of the salient points with respect to the subject. Our network supports deep supervision and is trainable end-to-end. Furthermore, our network is groundbreaking in its approach, as it addresses the task of modelling the likelihood of a subject's gaze location within the scene as if it were a scene segmentation problem.

3.2. Multi-Modal Fusion (MMF) module

The MMF network, f_{mm} is shown in Figure 3. It outputs a heatmap $H_i \in \mathbb{R}^{H_i \times W_i}$ reflecting the probability of the gaze fixation point for a subject within the scene. We utilize the scene image I_i , the depth map D_i , the cropped face F_i , the binary face position mask M_i , and the DISM map S_i to identify the gaze target. We can represent the network f_{mm} mathematically as:

$$H_i = f_{mm}(I_i, D_i, M_i, F_i, S_i) \quad (6)$$

where S_i is obtained from the DISM network f_{ds} in Equation (3).

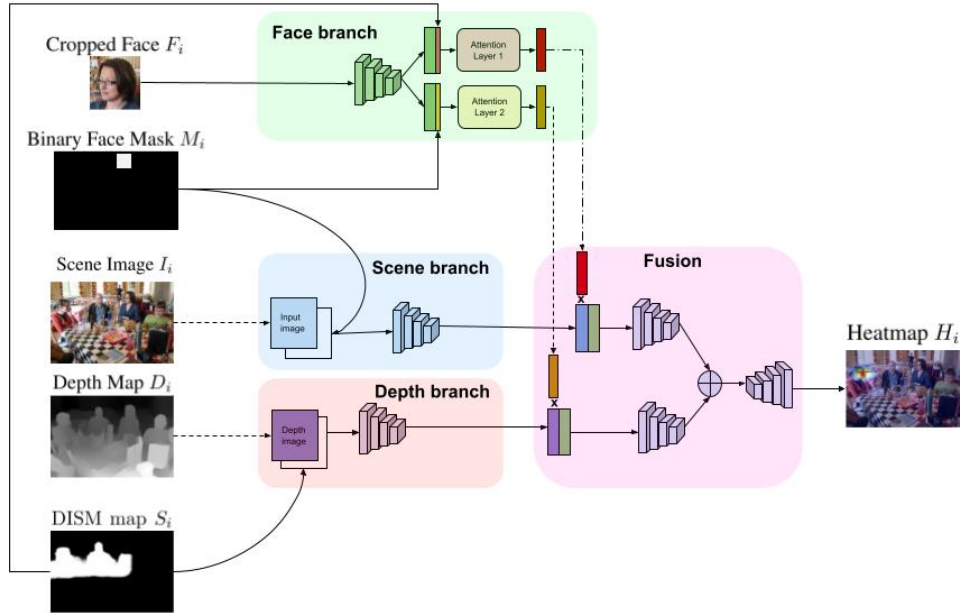


Figure 3: Our MMF module comprises three branches - face, scene, and depth. The three branches are fused in the Fusion module. The output of the module is a 2D Heatmap H_i superimposed on the scene image I_i here for visualization.

Face Branch f_f extracts facial features of dimension $1024 \times 7 \times 7$ from the cropped face image F_i using the face backbone. It then average-pools the extracted features to e_i^F , which has dimensions $1024 \times 1 \times 1$. e_i^F is then separately processed using a set of linear projections to learn the attention weights. Attention Layer 1 embeds the depth relevance by concatenating e_i^F with the max-pooled and flattened DISM map e_i^S , which represents the salient depth information in the scene. Attention Layer 2 embeds the spatial relevance of

the face by concatenating e_i^F with the max-pooled and flattened binary face position mask e_i^M . Both attention layers ($attn_i^S$ and $attn_i^M$) are represented as a set of linear projections f_S and f_M , respectively. These linear layers are then passed through a softmax function that applies weightage to spatial and depth-relevant cues within the image.

$$\begin{aligned} attn_i^S &= \Phi(f_S(e_i^F \oplus e_i^S)) \\ attn_i^M &= \Phi(f_M(e_i^F \oplus e_i^M)) \end{aligned} \quad (7)$$

where \oplus denote concatenation operation and Φ denote softmax function.

Scene Branch f_s branch takes as input the scene image I_i and the binary face position mask M_i . The two inputs are concatenated and passed through the scene backbone to extract the scene embedding e_i^I , where each embedding has a dimension of $1024 \times 7 \times 7$. e_i^I is then modulated by $attn_i^S$. The dimension of $attn_i^S$ is $1 \times 7 \times 7$. The modulated scene embedding e_i^{I*} has a dimension of $1024 \times 7 \times 7$ and is given by :

$$e_i^{I*} = e_i^I \otimes attn_i^S \quad (8)$$

Depth Branch f_d takes the depth map D_i and DISM map S_i as inputs. The two inputs are concatenated and passed through the depth network backbone. The output depth embedding e_i^D from the network has a dimension of $1024 \times 7 \times 7$. The depth embeddings are also modulated by $attn_i^M$ having a dimension of $1 \times 7 \times 7$. The modulated depth embedding e_i^{D*} with the dimension of $1024 \times 7 \times 7$ is given by :

$$e_i^{D*} = e_i^D \otimes attn_i^M \quad (9)$$

where \otimes represents elementwise multiplication operation.

The modulated scene embeddings e_i^{I*} and depth embeddings e_i^{D*} are concatenated with face embeddings e_i^F and are separately encoded using scene and depth encoders f_e^I and f_e^D . The encodings are fused by summation and finally passed on to a decoder f_d for predicting the gaze target heatmap H_i . The MMF network f_{mm} can thus alternatively be represented as :

$$H_i = f_{mm}(I_i, D_i, M_i, F_i, S_i) = f_d [f_e^I(e_i^{I*} \oplus e_i^F) + f_e^D(e_i^{D*} \oplus e_i^F)] \quad (10)$$

The ground-truth gaze heatmap, \hat{H}_i is attained by overlaying a Gaussian weight centred around the target gaze point. The objective of the network is to minimize the Heatmap Loss L_h which is computed using Mean Squared Error (MSE) loss for cases when the gaze target is present inside the frame for N instances within the dataset.

$$L_h(H_i, \hat{H}_i) = \sum_{i=1}^N (H_i - \hat{H}_i)^2 \quad (11)$$

3.3. Implementation Details

We have implemented the training and inferencing pipeline of our model using the PyTorch framework. All inputs are normalized and resized to 224×224 pixels. DISM uses a Resnet-101 (He et al., 2015) backbone pre-trained on ImageNet (Russakovsky et al., 2015). It has

a 5-stage encoder design with 256 and 128 convolution filters in the FPN feature pyramid and segmentation blocks, respectively. All backbones in the MMF module are pre-trained similar to Chong et al. (2018), Chong et al. (2020) and Fang et al. (2021). The scene and depth backbones were pre-trained on the Places dataset (Zhou et al., 2014), and the head backbone was pre-trained on the Eyediap dataset (Funes Mora et al., 2014). The face, scene, and depth feature extractors use Resnet-50 (He et al., 2015) backbones. The network outputs a 64×64 gaze heatmap. We use random crop, colour manipulation, random flip, and head bounding box jittering for data augmentation during training. We train the DISM and MMF module on GazeFollow (Recasens* et al., 2015) until convergence; then fine-tune on VideoAttentionTarget (Chong et al., 2020). We also train the network from scratch on the GOO-Real (Tomas et al., 2021) dataset. We use the Adam optimizer (Kingma and Ba, 2014) with a learning rate of 0.00025 and a batch size of 48.

4. Experiments

We quantitatively and qualitatively evaluated our full model on the VideoAttentionTarget, GazeFollow and GOO-Real datasets. We followed the standard training/testing splits of all datasets for a fair evaluation. We demonstrate that our method surpassed the performance of prior methods across most metrics in Section 4.3. Moreover, we perform an ablation study in Section 4.4 to validate the effectiveness of each module within our architecture.

4.1. Datasets

VideoAttentionTarget dataset comprises 164,541 frame-level head bounding boxes with 109,574 in-frame gaze targets and 54,967 out-of-frame gaze annotations. 10 shows were kept aside as test split, which comprises of 31,978 gaze annotations. **GazeFollow** dataset comprises of 122,143 images and about 160,000 annotations of people head bounding boxes and their corresponding gaze points. **Gaze On Objects (GOO)** dataset focuses on the retail environment where several grocery items are placed on shelves to imitate a real grocery store. GOO comprises 192,000 synthetic images (*GOO-Synth*) and 9552 real images (*GOO-Real*).

4.2. Evaluation Metrics

We use three evaluation metrics in line with previous works such as Chong et al. (2018, 2020); Fang et al. (2021); Recasens* et al. (2015); Lian et al. (2019); Tonini et al. (2022) to assess our model’s performance. In the GazeFollow dataset, the ground truth gaze target location is estimated by taking the average of the annotations provided by 10 different human annotators for each image and subject. **Area Under Curve (AUC):** We compare the flattened output gaze heatmap to the flattened binarized ground truth heatmap and plot the ROC curve using True Positive Rate and False Positive Rate. The AUC score is the area under this curve, with a score of 1.0 denoting perfect agreement of the prediction with the ground truth. **L2 Distance(Dist.):** The Euclidean distance between the ground truth target location and prediction heat map maximum is measured after normalizing the image height and width to 1. For the GazeFollow dataset, we also calculate the minimum distance (Min. Dist.) between the predicted gaze point and the 10 ground truth gaze target points for each subject. **Angular error(Ang.):** This metric reports the angular difference

between the predicted gaze direction and the ground truth gaze vector between face location and gaze point. We report all results from our experiments in Table 1 and Table 2.

4.3. Multi-Modal Saliency and Fusion Model Evaluation

We compare our model to several state-of-the-art architectures (Chong et al., 2020) (Recasens* et al., 2015) (Lian et al., 2019) (Chong et al., 2018) (Fang et al., 2021) (Jin et al., 2022) (Bao et al., 2022) (Tonini et al., 2022) for in-frame gaze target detection. We observed that the overall performance of our model is better on VideoAttentionTarget and GOO-Real, which have higher-resolution images than GazeFollow. The improved resolution translates to better depth map representations and generation of more accurate DISM maps from the 3D projections. See Figure 4 for visualizations of depth maps, DISM maps, MMF heatmaps, and predicted gaze target points for example cases from different datasets.

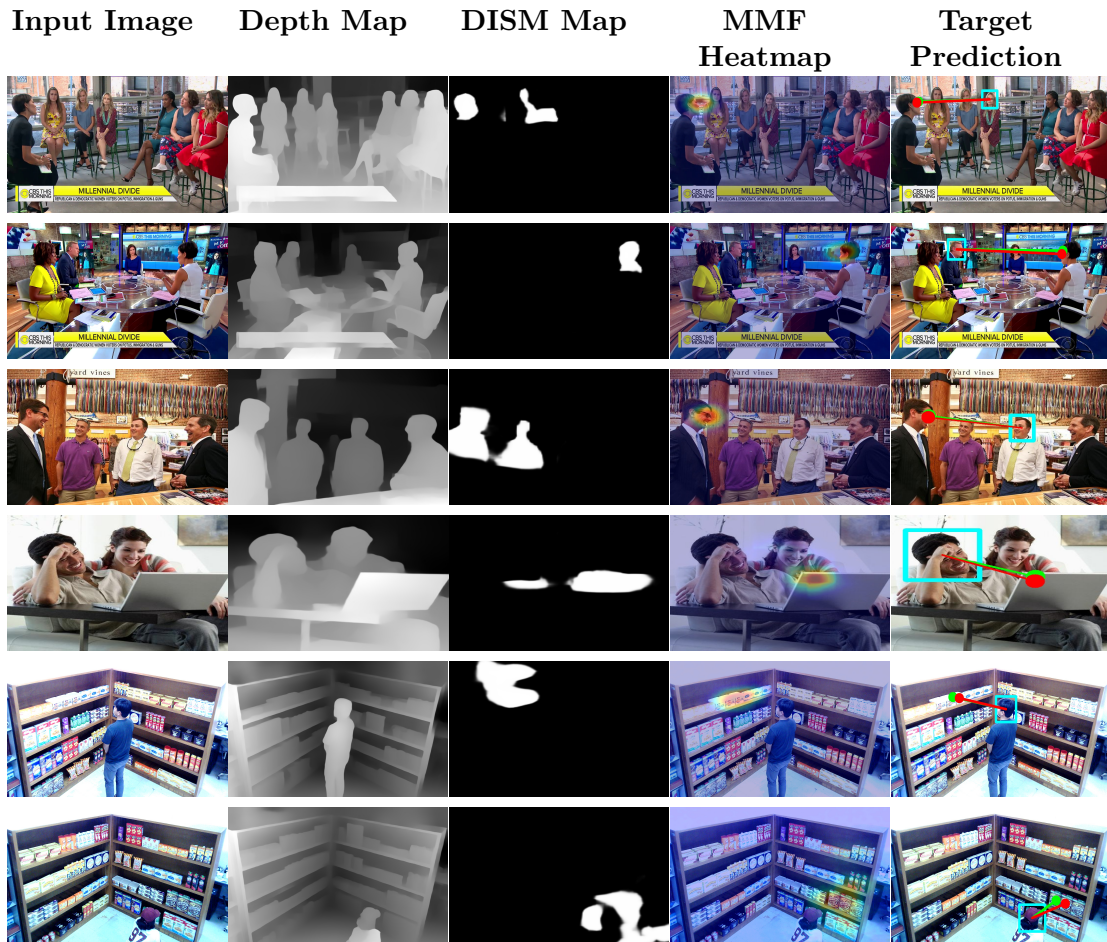


Figure 4: **Visualization results.** This figure shows examples from the VideoAttention-Target (first two rows), GazeFollow (middle two rows), and GOO-Real (last two rows) datasets. Each row shows the input image, depth map, DISM map, MMF heatmap, prediction result, and ground truth.

4.3.1. EVALUATION ON VIDEOATTENTIONTARGET

Quantitative results on VideoAttentionTarget dataset are summarized in Table 1. *Random* denotes that the prediction is made with 50% chance by sampling the values randomly from a Gaussian distribution. In *Fixed bias*, the bias present in the dataset in terms of position of the faces and the relative gaze fixation points are taken into consideration. It is to be noted that the method in Chong et al. (2020) uses a spatio-temporal architecture for video-based prediction (denoted as VideoAttn). For fair comparisons, we also include the performance of its spatial-only counterpart (denoted as VideoAttn[†]).

Ours[‡] refer to the GazeFollow-trained model (no fine-tuning) and **Ours** refer to the GazeFollow-trained model that is fine-tuned on VideoAttentionTarget. It is interesting to note that the performance of our model surpasses the performance of Chong et al. (2020) without the inclusion of any temporal features for video-based gaze target detection. Our proposed architecture also exhibits impressive generalization capabilities. The model trained purely on GazeFollow (**Ours[‡]**) outperforms all other state-of-the-art architectures that were finetuned on VideoAttentionTarget in the *AUC* metric. Finally, the fine-tuning of our model on VideoAttentionTarget (**Ours**) results in new state-of-the-art scores for both *AUC* and *Dist.* metrics. Some qualitative images are shown in Figure 5.

Table 1: Evaluation on VideoAttentionTarget and Goo-Real. * indicates taken from Tomas et al. (2021). The best and second-best scores are highlighted in **teal** and **red**.

Method	VideoAttentionTarget		GOO-Real	
	AUC↑	Dist.↓	AUC↑	Dist. ↓
Random (Chong et al., 2020)	0.505	0.458	-	-
Fixed Bias (Chong et al., 2020)	0.728	0.326	-	-
Recansens et al. (Recasens* et al., 2015)	-	-	0.850*	0.220*
Lian et al. (Lian et al., 2019)	-	-	0.840*	0.321*
Chong et al. (Chong et al., 2018)	0.830	0.193	-	-
VideoAttn [†] (Chong et al., 2020)	0.854	0.147	-	-
VideoAttn (Chong et al., 2020)	0.860	0.134	0.796*	0.252*
Danyang et al. (Tu et al., 2022)	0.893	0.137	-	-
Fang et al. (Fang et al., 2021)	0.905	0.108	-	-
Jin et al. (Jin et al., 2022)	0.901	0.116	-	-
Bao et al. (Bao et al., 2022)	0.885	0.120	-	-
Tonini et al. (Tonini et al., 2022)	0.940	0.129	0.918	0.164
Ours[‡]	0.958	0.123	0.876	0.208
Ours	0.964	0.100	0.954	0.130
Human	0.921	0.051	-	-

4.3.2. EVALUATION ON GOO-REAL

Similar to the notation scheme above, **Ours[‡]** denote the performance of the model trained on GazeFollow and tested on GOO-Real. The performance of the model trained from scratch

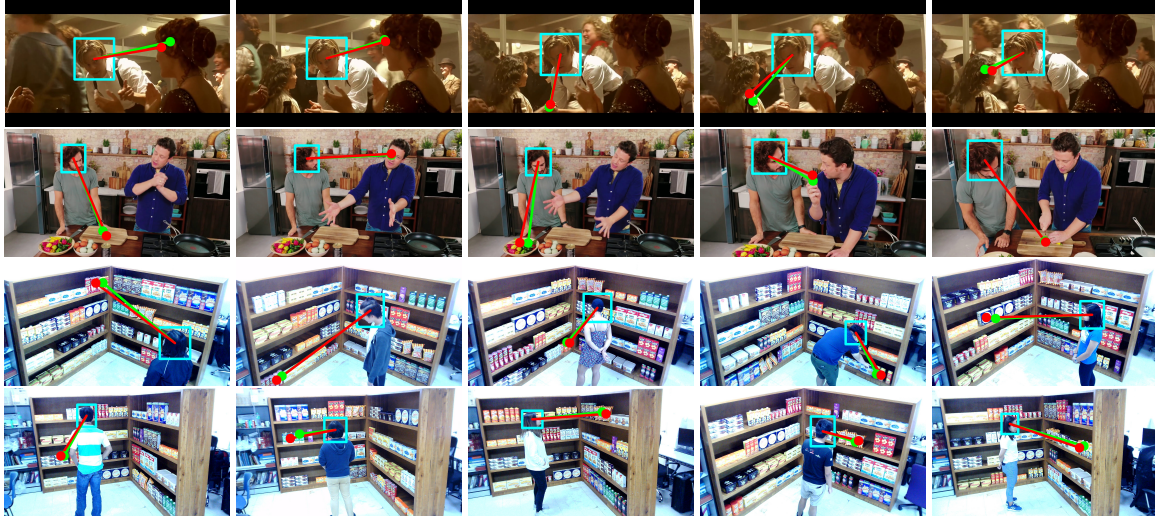


Figure 5: **Qualitative results.** The red and green lines denote [ground truth](#) and [predictions](#) respectively. The first two rows represent the changes in gaze target points of a subject from video sequences in VideoAttentionTarget. The last two rows are images from GOO-Real for varying head poses.

on GOO-Real is denoted as **Ours**. The authors of [Tomas et al. \(2021\)](#) trained and tested the architectures from [Recasens* et al. \(2015\)](#), [Lian et al. \(2019\)](#) and [Chong et al. \(2020\)](#) on GOO-Real dataset. The performance of these models is reported in Table 1. Our model trained on GazeFollow (**Ours[‡]**) was able to surpass the performance of [Recasens* et al. \(2015\)](#), [Lian et al. \(2019\)](#) and [Chong et al. \(2020\)](#) when tested on GOO-Real for both AUC and Dist. metrics even-though the model was not finetuned for retail gaze target detection using GOO-Real dataset. The model that was trained and tested on GOO-Real (**Ours**) sets the new benchmarks for both the AUC and Dist. metrics. Some qualitative images are shown in Figure 5.

4.3.3. EVALUATION ON GAZE FOLLOW

The quantitative results for the GazeFollow dataset are shown in Table 2. The entry labelled *Center* denotes the metrics are calculated by considering the gaze point to always be at the center of the image. Our model achieves new state-of-the-art in the AUC metric. Similar to [Bao et al. \(2022\)](#), we believe that *AUC* is a better metric than *Dist.* and *Angle* for the GazeFollow dataset because the latter metrics are susceptible to errors introduced by averaging human annotations. For example, Figure 6 shows how averaging human annotations can lead to inconsistent estimates of the ground-truth gaze target point. Our example case highlights that averaging the human annotations causes the gaze point to drift away from the true gaze point and causes the averaged gaze point not to be consistently centred around the object that the person is looking at. We additionally include some challenging scenarios and failure cases from GazeFollow dataset in Figure 6. Our model generalises

Table 2: Evaluation on GazeFollow dataset

Method	AUC↑	Dist.↓	Min. Dist.↓	Angle↓
Random	0.504	0.484	0.391	69.0
Center	0.633	0.313	0.230	49.0
Fixed bias	0.674	0.306	0.219	48.0
Recansens et al. (Recansens* et al., 2015)	0.878	0.190	0.113	24.0
Chong et al. (Chong et al., 2018)	0.896	0.187	0.112	-
Lian et al. (Lian et al., 2019)	0.906	0.145	0.081	17.6
Danyang et al. (Tu et al., 2022)	0.917	0.133	0.069	-
VideoAttn [†] (Chong et al., 2020)	0.921	0.137	0.077	-
Fang et al. (Fang et al., 2021)	0.922	0.124	0.067	14.9
Jin et al. (Jin et al., 2022)	0.923	0.120	0.064	14.8
Tonini et al. (Tonini et al., 2022)	0.927	0.141	-	-
Bao et al. (Bao et al., 2022)	0.928	0.122	-	14.6
Ours	0.932	0.133	0.073	19.3
Human	0.924	0.096	0.040	11.0

well and identifies the correct target gaze heatmap bin consistently, thus achieving new state-of-the-art scores on the AUC metric.

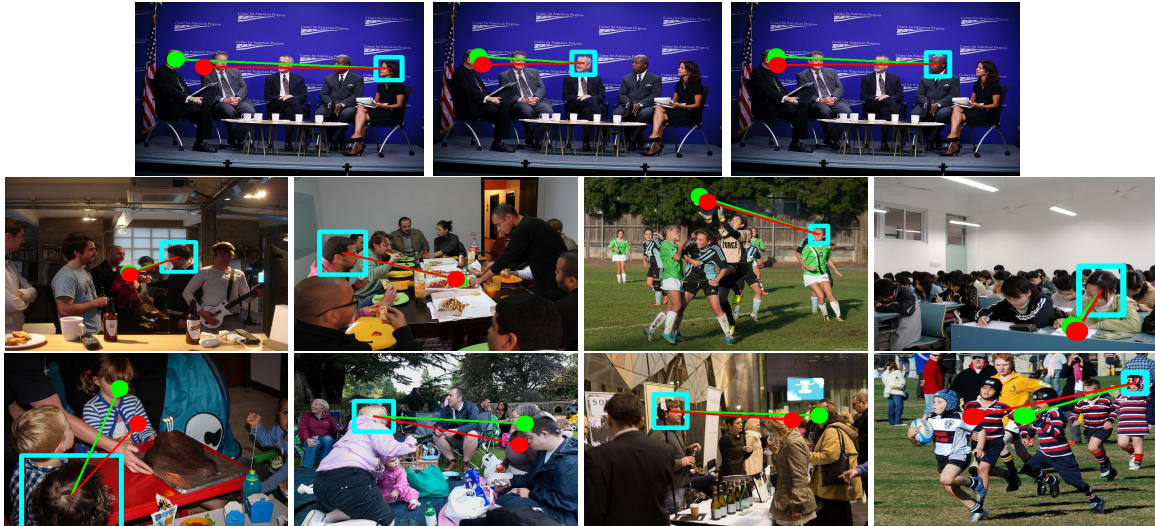


Figure 6: **Qualitative results.** Red, green and blue denote [average human annotation](#), [prediction](#), and [head location](#), respectively. The first row shows inconsistent human annotation, while our model predicts the same gaze target for all three subjects. The second row shows our model’s performance in challenging scenarios with complex backgrounds. The last row shows some failure cases, however, the predicted gaze targets contextually remain acceptable.

4.4. Ablation Study

In order to better understand the impact of various components within our system, we conducted further analysis using the GOO-Real dataset. Firstly, we removed the attention layers $attn_i^M$ and $attn_i^S$ from the network. This is reflected as injecting e_i^D instead of e_i^{D*} into f_e^D and e_i^I instead of e_i^{I*} into f_e^I (Attention-None). Next, we removed the DISM map, S_i , and replaced it with a uniformly weighted mask (DISM-None). We then removed all inputs in relation to the depth map D_i . We removed the Depth branch and $attn_i^S$ which modulates the scene embedding e_i^I based on DISM map which is inherently learned from the depth map (Depth - None). Finally, we removed the Scene branch. This means that only the output of the depth encoder f_e^D is fed to the decoder f_d (Scene-None). We also evaluated the multi-modal fusion module using ground-truth DISM maps (DISM pseudo-labels). The results, sorted in the order of their performance are reported in Table 3. We notice that DISM contributes significantly to the overall model performance. We also show that all components of our network are necessary to attain exceptional performance.

Table 3: Ablation study on GOO-Real dataset

Method	AUC↑	Dist.↓
DISM - None	0.911	0.188
Depth - None	0.915	0.186
Scene - None	0.941	0.140
Attention - None	0.948	0.135
Ours - All (DISM pseudo-labels)	0.959	0.128
Ours - All	0.954	0.130

5. Conclusion

In this research, we have presented a GTD architecture comprising two key modules: Depth-Infused Saliency and Multi-Modal Fusion. The former focuses on identifying salient artefacts relevant to the subject within the scene image to generate the DISM map and the latter leverages the generated DISM map while fusing multiple modalities to generate the gaze target heatmap. This approach has proven to outperform similar contemporary research in terms of various state-of-the-art metrics. We presented challenging scenarios and failure cases to our model to test its generalization capabilities and it consistently pinpointed the gaze target correctly. This research represents a significant step forward in gaze target detection, offering a robust and effective approach to understanding human gaze within complex scenes.

6. Future Work

One of our next goals is to improve our network with a dedicated component for out-of-frame gaze detection. Furthermore, we envision extending our work into the field of education, aiming to enhance student-teacher interaction and engagement. Such systems necessitate a robust face detector. This inspires us to explore transformer-based networks and self-attention mechanisms, to concurrently identify faces and their associated gaze points.

References

Karan Ahuja, Deval Shah, Sujeath Pareddy, Franceska Xhakaj, Amy Ogan, Yuvraj Agarwal, and Chris Harrison. Classroom digital twins with instrumentation-free gaze tracking. pages 1–9, 2021.

Jun Bao, Buyu Liu, and Jun Yu. Escnet: Gaze target detection with the understanding of 3d scenes. In *2022 IEEE/CVF Conference on Computer Vision and Pattern Recognition (CVPR)*, pages 14106–14115, 2022. doi: 10.1109/CVPR52688.2022.01373.

E. Chong, Y. Wang, N. Ruiz, and J. M. Rehg. Detecting attended visual targets in video. In *2020 IEEE/CVF Conference on Computer Vision and Pattern Recognition (CVPR)*, pages 5395–5405, Los Alamitos, CA, USA, jun 2020. IEEE Computer Society. doi: 10.1109/CVPR42600.2020.00544. URL <https://doi.ieeecomputersociety.org/10.1109/CVPR42600.2020.00544>.

Eunji Chong, Nataniel Ruiz, Yongxin Wang, Yun Zhang, Agata Rozga, and James M. Rehg. Connecting gaze, scene, and attention: Generalized attention estimation via joint modeling of gaze and scene saliency. In *Computer Vision – ECCV 2018: 15th European Conference, Munich, Germany, September 8–14, 2018, Proceedings, Part V*, page 397–412, Berlin, Heidelberg, 2018. Springer-Verlag. ISBN 978-3-030-01227-4. doi: 10.1007/978-3-030-01228-1_24. URL https://doi.org/10.1007/978-3-030-01228-1_24.

Yi Fang, Jiapeng Tang, Wang Shen, Wei Shen, Xiao Gu, Li Song, and Guangtao Zhai. Dual attention guided gaze target detection in the wild. In *2021 IEEE/CVF Conference on Computer Vision and Pattern Recognition (CVPR)*, pages 11385–11394, 2021. doi: 10.1109/CVPR46437.2021.01123.

Kenneth Funes Mora, Florent Monay, and Jean-Marc Odobez. Eyediap: a database for the development and evaluation of gaze estimation algorithms from rgb and rgb-d cameras. pages 255–258, 03 2014. doi: 10.1145/2578153.2578190.

S. Garrido-Jurado, R. Muñoz Salinas, F.J. Madrid-Cuevas, and M.J. Marín-Jiménez. Automatic generation and detection of highly reliable fiducial markers under occlusion. *Pattern Recogn.*, 47(6):2280–2292, jun 2014. ISSN 0031-3203. doi: 10.1016/j.patcog.2014.01.005. URL <https://doi.org/10.1016/j.patcog.2014.01.005>.

Xinwei Guo, Yong Wu, Jingjing Miao, and Yang Chen. LiteGaze: Neural architecture search for efficient gaze estimation. *PLOS ONE*, 18(5):e0284814–, 5 2023. URL <https://doi.org/10.1371/journal.pone.0284814>.

Kaiming He, Xiangyu Zhang, Shaoqing Ren, and Jian Sun. Deep residual learning for image recognition, 2015.

Qiong Huang, Ashok Veeraraghavan, and Ashutosh Sabharwal. Tabletgaze: Dataset and analysis for unconstrained appearance-based gaze estimation in mobile tablets. *Mach. Vision Appl.*, 28(5–6):445–461, aug 2017. ISSN 0932-8092. doi: 10.1007/s00138-017-0852-4. URL <https://doi.org/10.1007/s00138-017-0852-4>.

Laurent Itti and Christof Koch. Computational modelling of visual attention. *Nature reviews neuroscience*, 2(3):194–203, 2001.

Tianlei Jin, Qizhi Yu, Shiqiang Zhu, Zheyuan Lin, Jie Ren, Yuanhai Zhou, and Wei Song. Depth-aware gaze-following via auxiliary networks for robotics. *Engineering Applications of Artificial Intelligence*, 113:104924, 2022. ISSN 0952-1976. doi: <https://doi.org/10.1016/j.engappai.2022.104924>. URL <https://www.sciencedirect.com/science/article/pii/S0952197622001464>.

Tilke Judd, Krista Ehinger, Frédo Durand, and Antonio Torralba. Learning to predict where humans look. In *IEEE International Conference on Computer Vision (ICCV)*, 2009.

Diederik Kingma and Jimmy Ba. Adam: A method for stochastic optimization. *International Conference on Learning Representations*, 12 2014.

Kyle Kafka, Aditya Khosla, Petr Kellnhofer, Harini Kannan, Suchendra Bhandarkar, Wojciech Matusik, and Antonio Torralba. Eye tracking for everyone. In *IEEE Conference on Computer Vision and Pattern Recognition (CVPR)*, 2016.

Dongze Lian, Zehao Yu, and Shenghua Gao. Believe it or not, we know what you are looking at! In C. V. Jawahar, Hongdong Li, Greg Mori, and Konrad Schindler, editors, *Computer Vision – ACCV 2018*, pages 35–50, Cham, 2019. Springer International Publishing. ISBN 978-3-030-20893-6.

Tsung-Yi Lin, Piotr Dollár, Ross Girshick, Kaiming He, Bharath Hariharan, and Serge Belongie. Feature pyramid networks for object detection, 2017.

Meng Liu, Youfu Li, and Hai Liu. 3d gaze estimation for head-mounted eye tracking system with auto-calibration method. *IEEE Access*, 8:104207–104215, 2020.

Kristine Lund. The importance of gaze and gesture in interactive multimodal explanation. *Language Resources and Evaluation*, 41:289–303, 2007.

Daniel Parks, Ali Borji, and Laurent Itti. Augmented saliency model using automatic 3d head pose detection and learned gaze following in natural scenes. *Vision research*, 116: 113–126, 2015.

René Ranftl, Katrin Lasinger, David Hafner, Konrad Schindler, and Vladlen Koltun. Towards robust monocular depth estimation: Mixing datasets for zero-shot cross-dataset transfer, 2020.

René Ranftl, Alexey Bochkovskiy, and Vladlen Koltun. Vision transformers for dense prediction, 2021.

Adria Recasens*, Aditya Khosla*, Carl Vondrick, and Antonio Torralba. Where are they looking? In *Advances in Neural Information Processing Systems (NIPS)*, 2015. * indicates equal contribution.

Adria Recasens, Carl Vondrick, Aditya Khosla, and Antonio Torralba. Following gaze in video. In *Proceedings of the IEEE International Conference on Computer Vision*, pages 1435–1443, 2017.

Olga Russakovsky, Jia Deng, Hao Su, Jonathan Krause, Sanjeev Satheesh, Sean Ma, Zhiheng Huang, Andrej Karpathy, Aditya Khosla, Michael Bernstein, Alexander C. Berg, and Li Fei-Fei. ImageNet Large Scale Visual Recognition Challenge. *International Journal of Computer Vision (IJCV)*, 115(3):211–252, 2015. doi: 10.1007/s11263-015-0816-y.

Shashimal Senarath, Primesh Pathirana, Dulani Meedeniya, and Sampath Jayarathna. Retail gaze: A dataset for gaze estimation in retail environments. In *2022 International Conference on Decision Aid Sciences and Applications (DASA)*, pages 1040–1044. IEEE, 2022. ISBN 1665495014.

Kyuhong Shim, Jiyoung Kim, Gusang Lee, and Byonghyo Shim. Depth-Relative Self Attention for Monocular Depth Estimation. *arXiv preprint arXiv:2304.12849*, 2023.

Sanket Kumar Thakur, Cigdem Beyan, Pietro Morerio, and Alessio Del Bue. Predicting gaze from egocentric social interaction videos and imu data. In *Proceedings of the 2021 International Conference on Multimodal Interaction*, pages 717–722, 2021.

Henri Tomas, Marcus Reyes, Raimarc Dionido, Mark Ty, Joel Casimiro, Rowel Atienza, and Richard Guinto. Goo: A dataset for gaze object prediction in retail environments. In *CVPR Workshops (CVPRW)*, 2021.

Francesco Tonini, Cigdem Beyan, and Elisa Ricci. Multimodal across domains gaze target detection. In *International Conference on Multimodal Interaction*. ACM, nov 2022. doi: 10.1145/3536221.3556624. URL <https://doi.org/10.1145%2F3536221.3556624>.

Danyang Tu, Xiongkuo Min, Huiyu Duan, Guodong Guo, Guangtao Zhai, and Wei Shen. End-to-end human-gaze-target detection with transformers. In *2022 IEEE/CVF Conference on Computer Vision and Pattern Recognition (CVPR)*, pages 2192–2200. IEEE, 2022.

Xucong Zhang, Yusuke Sugano, Mario Fritz, and Andreas Bulling. Appearance-based gaze estimation in the wild. In *Proceedings of the IEEE conference on computer vision and pattern recognition*, pages 4511–4520, 2015.

Xucong Zhang, Michael Xuelin Huang, Yusuke Sugano, and Andreas Bulling. Training person-specific gaze estimators from user interactions with multiple devices. In *Proceedings of the 2018 CHI conference on human factors in computing systems*, pages 1–12, 2018.

Bolei Zhou, Agata Lapedriza, Jianxiong Xiao, Antonio Torralba, and Aude Oliva. Learning deep features for scene recognition using places database. In *Proceedings of the 27th International Conference on Neural Information Processing Systems - Volume 1*, NIPS’14, page 487–495, Cambridge, MA, USA, 2014. MIT Press.

Ömer Sümer, Patricia Goldberg, Sidney D'Mello, Peter Gerjets, Ulrich Trautwein, and Enkelejda Kasneci. Multimodal engagement analysis from facial videos in the classroom. *arXiv preprint arXiv:2101.04215*, 2021.